05,10

Influence of the magnetic field of a spin-polarized current on gyrotropic autooscillations of vortex nanooscillators

© D.A. Tatarskiy[1,2], O.L. Ermolaeva[1], V.L. Mironov[1], A.A. Fraerman[1]

[1] Institute of Physics of Microstructures, Russian Academy of Sciences, Nizhny Novgorod, Russia
[2] Lobachevsky State University, Nizhny Novgorod, Russia

E-mail: tatarsky@ipmras.ru

Received April 18, 2024
Revised April 18, 2024
Accepted May 8, 2024

The results of micromagnetic modeling of gyrotropic self-oscillations of a vortex spin-transfer nanooscillator (VSTN) taking into account the magnetic field of the pump current are presented. The dependences of the core orbital radius, resonant frequency, and gyration rate of the magnetic vortex on the pump current density are studied for different values of the ratio of the thickness of the VSTN stack to its diameter. It is shown that the gyration parameters depend significantly on the mutual direction of the vortex magnetic field and the magnetization in the shell of the magnetic vortex. The conditions for phase synchronization of magnetostatically coupled VSTN chains are discussed.

Keywords: magnetic vortex, vortex spin-transfer nanooscillators, Oersted magnetic field, phase synchronization.

DOI: 10.61011/PSS.2024.08.59042.56HH

1. Introduction

A low-frequency resonance associated with gyrotropic motion of the core of a magnetic vortex around the equilibrium position is found in circular ferromagnetic discs with a vortex magnetization state. This resonance was predicted theoretically [1,2] and investigated experimentally and via micromagnetic modeling [3–10]. The interest in the gyrotropic oscillation mode has been on the rise lately due to the development of vortex spin-transfer nanooscillators (VSTN) based on magnetic tunnel junction (MTJ), where the vortex magnetization state is used to generate high-frequency electromagnetic oscillations [11,12]. The electric current through MTJ is modulated in these structures by a rotating magnetic moment induced in a magnetic vortex with its core in circular motion. The use of an MTJ-based vortex nanooscillator with an MgO barrier makes it possible to reach fairly high microwave power levels (on the order of 10^{-5} W) [12]. To increase the generated power, VSTN are combined into arrays with oscillation synchronization by the magnetostatic [13–16] or exchange interaction [17–21]. However, one significant factor affecting the synchronization of VSTN is the spread of their partial frequencies that may be caused by the difference in a number of parameters, such as the tunnel barrier transparency, pump currents, or geometric parameters of discs in individual MTJ. The situation is aggravated further by the presence of magnetic fields induced by pump currents, which also leads to significant dephasing of VSTNs in an array. The influence of internal magnetic fields on the intrinsic frequencies of VSTNs was examined in [22–26], but their effect on the phase synchronization of VSTN remains unexplored. In the present study, the influence of the magnetic field produced by pump current on the parameters of gyrotropic oscillations of a magnetic vortex and on the phase synchronization of magnetostatically coupled VSTN is investigated via micromagnetic modeling.

2. Methods

Magnetization changes under the influence of spin-polarized current were modeled by numerical integration of the Landau–Lifshitz–Gilbert–Slonczewski equation for the magnetic moment

$$\frac{\partial \mathbf{m}}{\partial t} = -\frac{|\gamma|}{1+\alpha^2}\left[\mathbf{m}\times\mathbf{H}_{\text{eff}}\right] + \mathbf{T}_d + \mathbf{T}_s, \qquad (1)$$

where $\mathbf{m}$ is a unit vector in the direction of magnetization, γ is the gyromagnetic ratio, and α is a dimensionless parameter that characterizes damping. Effective magnetic field $\mathbf{H}_{\text{eff}}$ is written as

$$\mathbf{H}_{\text{eff}} = \mathbf{H}_{\text{ex}} + \mathbf{H}_{\text{dem}} + \mathbf{H}_{\text{cur}}, \qquad (2)$$

where $\mathbf{H}_{\text{ex}}$ is the exchange field, $\mathbf{H}_{\text{dem}}$ is the demagnetizing field due to magnetization, and $\mathbf{H}_{\text{cur}}$ is the field of spin-polarized pump current (Oersted field). The term characterizing the damping of precession has the following form:

$$\mathbf{T}_d = -\frac{|\gamma|}{1+\alpha^2}\left[\mathbf{m}\times\left[\mathbf{m}\times\mathbf{H}_{\text{eff}}\right]\right]. \qquad (3)$$

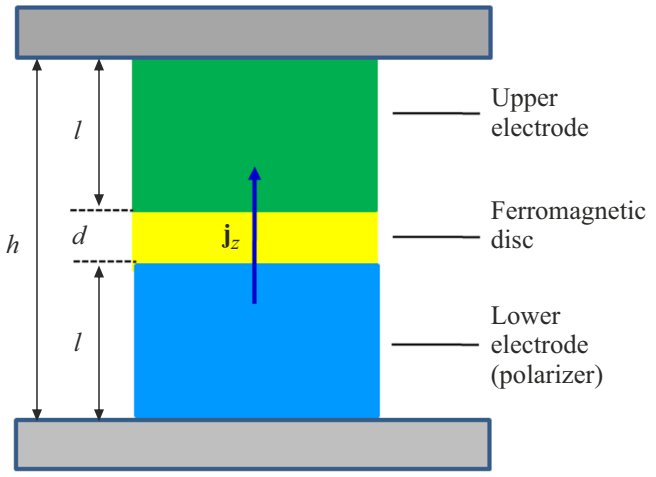

Figure 1. Schematic diagram of a magnetic nanocontact.

The term characterizing the spin-torque effect is written as [27,28]

$$\mathbf{T}_s = \beta \frac{\varepsilon}{1+\alpha^2}\left[\mathbf{m}\times[\mathbf{m}_p\times\mathbf{m}]\right] + \beta\frac{\alpha\varepsilon}{1+\alpha^2}[\mathbf{m}_p\times\mathbf{m}]. \quad (4)$$

Here, $\mathbf{m}_p$ is the magnetic moment of the polarizer and

$$\beta = \frac{j_z\hbar}{M_{\text{sat}}e\delta},$$

where j_z is the current density along axis Z perpendicular to the surface of discs, $\hbar$ is the Planck constant, M_{sat} is the saturation magnetization, e is the electron charge, and δ is the injector layer thickness. Parameter ε is given by

$$\varepsilon = \frac{P\Lambda^2}{(\Lambda^2+1)+(\Lambda^2-1)(\mathbf{m}\cdot\mathbf{m}_p)}, \quad (5)$$

where P is the degree of polarization of charge carriers and parameter Λ is related to the tunnel barrier conductance [29].

A tunnel magnetic contact of finite thickness (Figure 1) was considered in the present study. The layer with a vortex magnetization pattern is highlighted in the figure; the other layers, such as the carrier polarizer and polarization analyzer and the tunnel layer, are part of the corresponding electrodes. Field $\mathbf{H}_{\text{cur}}$ of the pump current may be calculated only numerically in this case on the basis of the Bio–Savart–Laplace law. It was assumed that homogeneous electric current flows through a cylinder with height h and radius $r = 250\,\text{nm}$. The magnetic field of current was calculated using the Wolfram Mathematica package on a rectangular grid with $31.25\times31.25\times5\,\text{nm}^3$ in size. The obtained field distribution was then transferred by interpolation to a grid that matched the numerical grid of micromagnetic modeling. It was also assumed that the configuration of supply wires is such that their magnetic fields compensate each other.

The MuMax^3 simulator [27] was used to solve Eq. (1) numerically. A circular permalloy disc with radius $r = 250\,\text{nm}$ and thickness $d = 20\,\text{nm}$ was chosen as the basic element for modelling. The following material parameters were used in calculations: saturation magnetization $M_{\text{sat}} = 800\,\text{kA/m}$, exchange interaction constant $J = 13\cdot10^{-12}\,\text{J/m}$, damping parameter $\alpha = 0.01$, anisotropy constant $K = 0$, and parameters $P = 0.2$ and $\Lambda = 1$. A $128\times128\times1$ ($512\times128\times1$) grid with a $4\times4\times20\,\text{nm}^3$ unit cell, which is smaller in lateral dimensions than exchange length $l_{\text{ex}}\approx5.7\,\text{nm}$ [30], was used to model a single disc (chain of discs). The cell height was equal to the disc thickness [31]. Periodic boundary conditions in the corresponding direction were applied in modeling of a disc chain.

In order to induce gyrotropic self-oscillations, the vortex equilibrium was first disturbed by applying a weak magnetic field (10 Oe) in the disc plane, and then the pump current was switched on and the field was switched off. When a chain of discs was modeled, 20 Oe were also applied to each disc at the initial stage. The local fields in discs were directed at an angle of 85° to exclude the generation of an antiphase mode of self-oscillations or „instantaneous“ synchronization.

3. Influence of the pump current field on the gyration of a magnetic vortex in a nanooscillator

Let us consider the effect of the magnetic field of the pump current on a single vortex nanooscillator. The schematic diagram of a cylindrical magnetic nanocontact is shown in Figure 1. Symmetric nanocontacts with a ferromagnetic working layer with thickness d located in the middle were examined:

$$h = d + 2l,$$

where l is the thickness of the upper and lower electrodes. The total electrode thickness was $L = 2l$.

Spin-polarized current flowing through a nanooscillator produces magnetic field $\mathbf{H}_{\text{cur}}$, which affects the gyration parameters of a magnetic vortex. The dependence of the azimuthal projection of the magnetic field $(H_\phi/j_z/H_0)$ at the edge of a disc with $r = 250\,\text{nm}$ normalized both to current density $j_z = 10^7\,\text{A/cm}^2$ and to magnetic field $H_0\approx150\,\text{Oe}$ of current in an infinite conductor on normalized nanocontact thickness (h/r) is shown in Figure 2.

As the thickness of the supply electrodes increases, the magnetic field at the disc edge intensifies monotonically, reaching 87% of the magnitude of the infinite wire field at $h/r = 5$.

The magnetic field of pump current affects significantly the parameters of gyrotropic oscillations of a magnetic vortex. The dependences of critical currents and the frequency of self-oscillations of a magnetic vortex on the supply electrode thickness are presented in Figure 3. If one

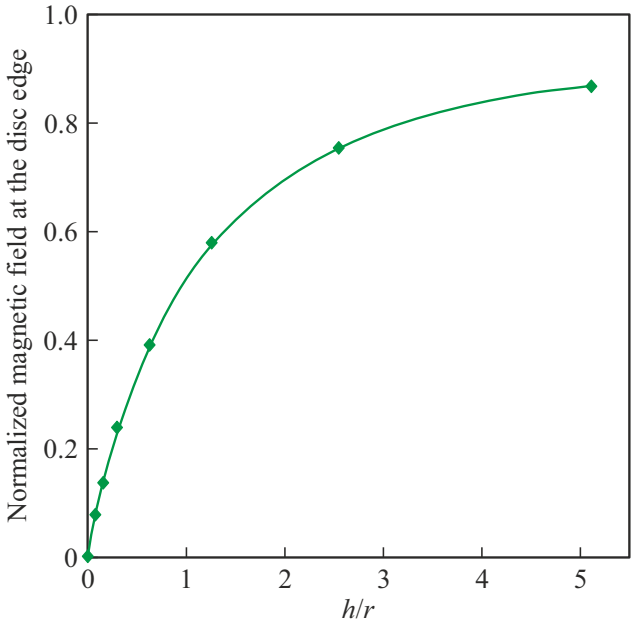

Figure 2. Dependence of the magnetic field at the disc edge on the proportions of supply electrodes.

disregards the magnetic field, the critical current density of the start of self-oscillations is $j_{\text{Start}} = 1.067 \cdot 10^7$ A/cm^2, and the current density reached when oscillations stop is $j_{\text{Stop}} = 1.628 \cdot 10^7$ A/cm^2. The magnetic field of current induces a shift of these parameter values. When the vortex shell vorticity is co-directional with the magnetic field of current (H^+/V^+), the values of parameters j_{Start} and j_{Stop} increase. The resonant frequency of self-oscillations also grows from 340 to 440 MHz. When the vorticity is directed opposite to the magnetic field (H^+/V^-), the values of j_{Start} and j_{Stop} decrease, and the resonant frequency drops from 340 to 280 MHz.

Figure 4 presents diagrams illustrating the dependence of the steady orbit radius of a vortex core on thickness of the supply electrodes and pump current magnitude. It can be seen that the vortex core orbit radius in the H^+/V^- case is greater than the one in state H^+/V^+.

At the same time, it was found in modeling that the gyration rate of the vortex core is virtually independent of the mutual orientation of the magnetic field and the vortex shell vorticity. Diagrams illustrating the dependence of the vortex gyration rate on thickness of the supply electrodes and pump current magnitude are shown in Figure 5. The minimum gyration rates in these diagrams are on the order of 20 m/s, while the maximum rates are close to 340 m/s. This depicted in greater detail in Figure 6, which shows the cross sections of diagrams from Figures 3–5 corresponding to different values of parameter h/r. Figure 6 demonstrates that orbit radius r_g increases monotonically with increasing pump current (Figure 6, a), while self-oscillation frequency ω_g increases at first, but then decreases (Figure 6, b). However, linear vortex gyration rate v_g is virtually independent of parameter h/r (Figure 6, c) and is calculated as

$$v_g = r_g \omega_g.$$

The reduction in gyration frequency with an increase in pump current is apparently attributable to the transformation of the vortex core in large gyration orbits. It is known that the so-called „anti-core“ (region with magnetization directed opposite to that of the core) starts forming near the vortex core at pump currents close to j_{Stop}, eventually inducing a switch of the core polarity and suppressing gyration [32]. The calculated profiles of the Z-projection of magnetization in the radial section of a magnetic vortex at different pump

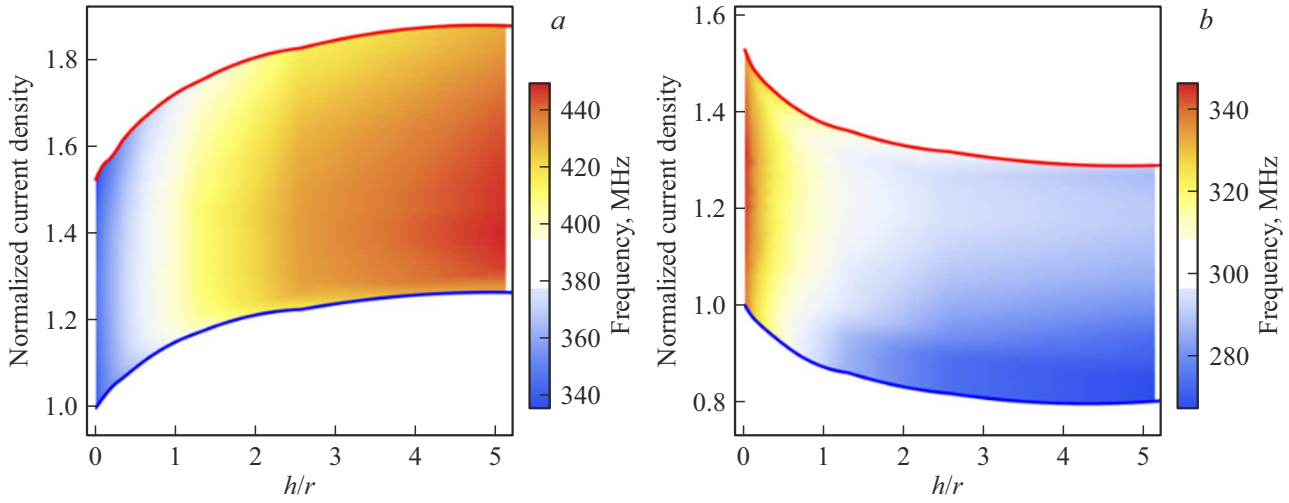

Figure 3. Dependences of the critical current densities and the frequency of magnetic vortex self-oscillations on the proportions of supply electrodes. a) Vorticity direction matches the magnetic field direction (H^+/V^+); b) vorticity is directed opposite to the field (H^+/V^-). The lower bounds (blue curves) correspond to the current density of the start of generation, while the upper bounds (red curves) represent the current density at the moment when generation stops. Current densities are normalized to $j_{\text{Start}} = 1.067 \cdot 10^7$ A/cm^2.

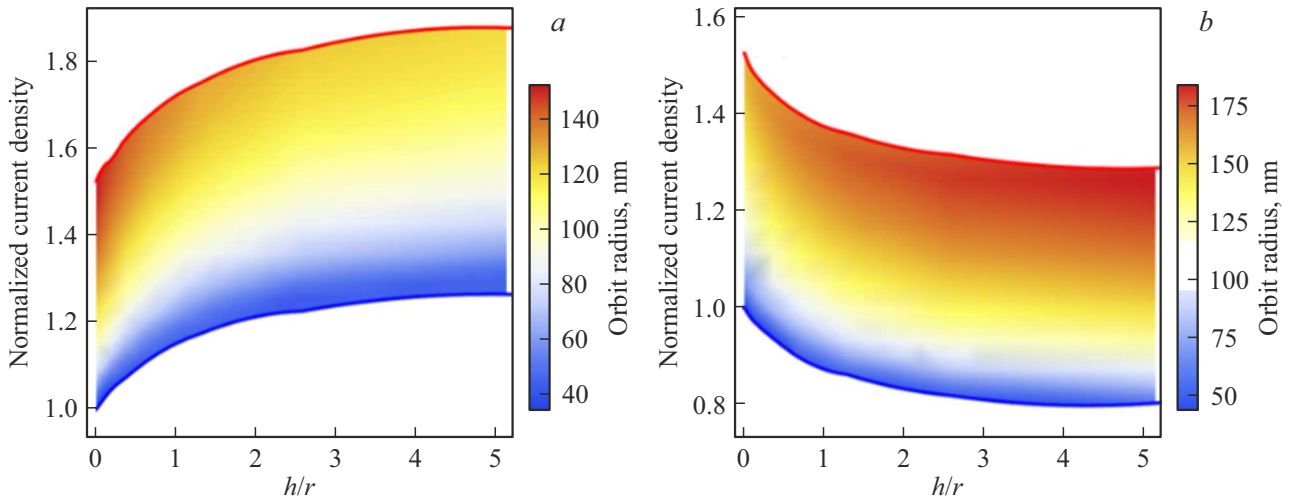

Figure 4. Dependences of the steady orbit radius of a vortex core (color gradient) on the proportions of supply electrodes and the pump current density: *a*) state (H^+/V^+); *b*) state (H^+/V^-). Current densities are normalized to $j_{\text{Start}} = 1.067 \cdot 10^7$ A/cm^2.

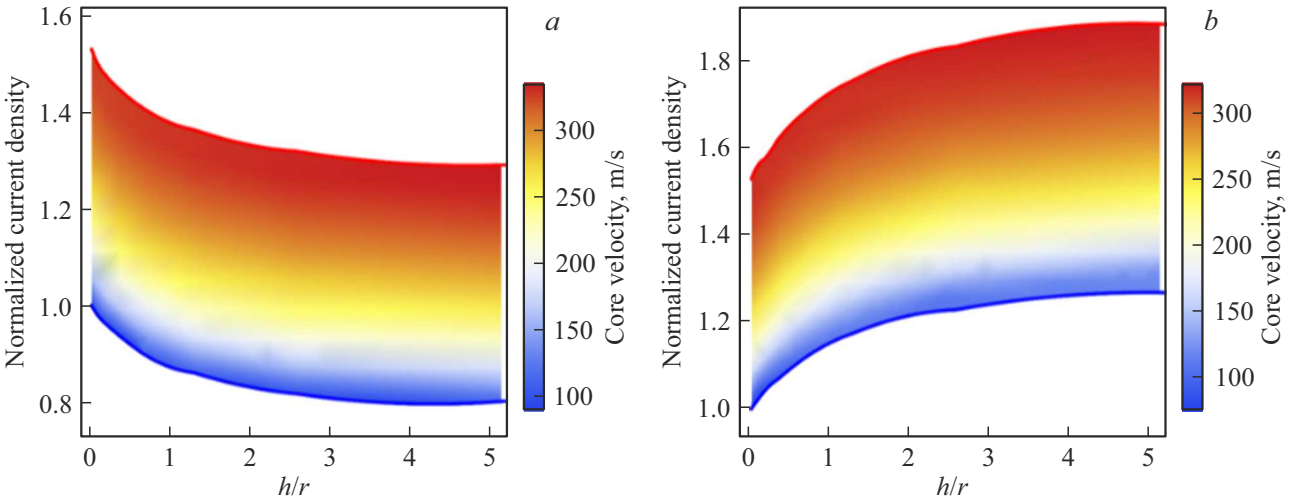

Figure 5. Dependences of the vortex gyration rate (color gradient) on the proportions of supply electrodes and the pump current density: *a*) state (H^+/V^+); *b*) state (H^+/V^-). Current densities are normalized to $j_{\text{Start}} = 1.067 \cdot 10^7$ A/cm^2.

currents are shown in Figure 7, *a*. It can be seen that the amplitude of the anti-core peak increases with an increase in current density, while the core amplitude remains constant. The dependences of integral magnetic moments of the core and anti-core on pump current are shown in Figure 7, *b*. It is evident that the integral moment of the core remains virtually unchanged, whereas the magnetic moment of the anti-core increases by almost an order of magnitude, which leads to switching of the vortex polarity.

4. Influence of the pump current field on synchronization of nanooscillators

The features of synchronization of self-oscillations of vortices in discs combined into chains were examined. The dependences of the oscillation phase difference on the direction of shell vorticity of adjacent discs at different directions of pump currents were studied. Magnetic field distributions were calculated for nanocontacts with ratio $h/r = 0.3$ (which corresponds to contact thickness $h = 80$ nm) and pump current density $j = 1.1 \cdot 10^7$ A/cm^2. This current was chosen so as to fall within the $j_{\text{Start}}-j_{\text{Stop}}$ generation ranges for all possible combinations of directions of vortex shell vorticity and magnetic fields of current. Two methods of pumping the discs in a chain were considered. In the first method, the electric pump current had the same direction in adjacent discs, and magnetic field configuration H^+H^+ was established. In the second case, the currents were directed opposite to each other, and the configuration was H^+H^-. Figure 8 shows the magnetic field distributions in a unit cell of the disc chain. The field reaches its maximum at the disc edges. The fields in the region between

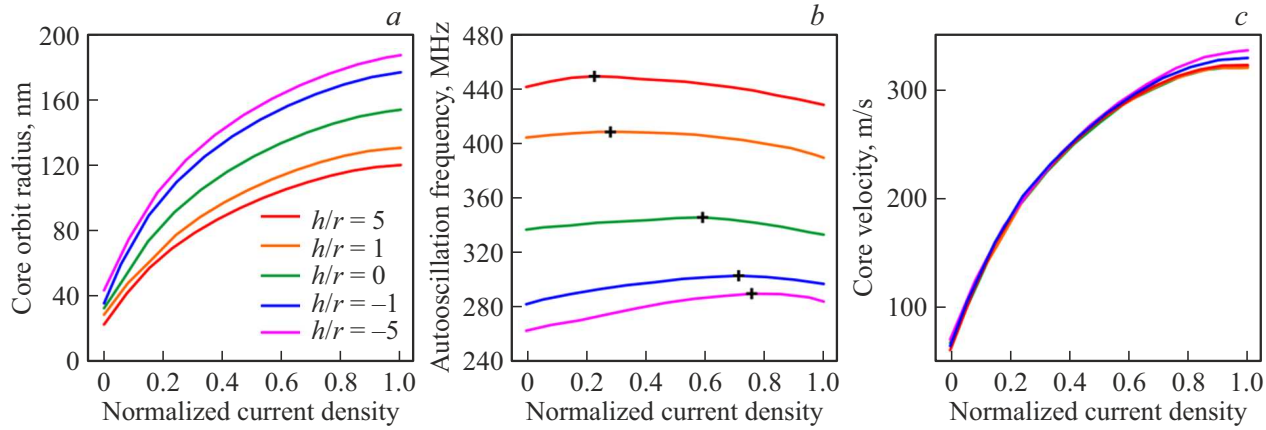

Figure 6. Dependences of a) core orbit radius, b) resonant frequency, and c) gyration rate of the vortex core on normalized pump current density $(j-j_{\text{Start}})/(j_{\text{Stop}}-j_{\text{Start}})$ at different values of ratio h/r. The „+“ and „–“ signs of the h/r ratio correspond to states H^+/V^+ and H^+/V^-. Crosses in panel (b/) denote local frequency maxima.

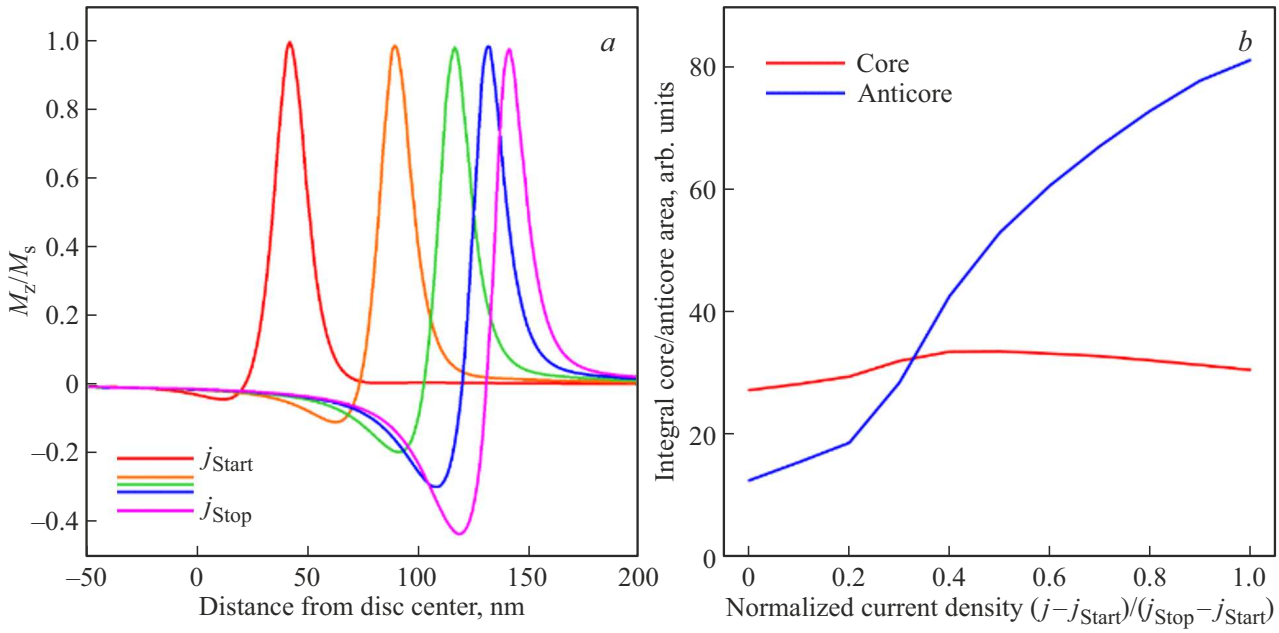

Figure 7. a) Distributions of the z magnetization component in the central section of a vortex at different pump current densities. b) Dependences of integral magnetizations of the core and „anti-core“ on pump current density at $h/r = 0.3$.

discs are compensated in configuration H^+H^+ (Figure 8, a) and are combined in the H^+H^- case.

Steady gyrotropic oscillations at a distance of $2r$ between the edges of discs were examined to analyze the phase characteristics of vortex gyration. Steady fluctuations of the phase difference of vortex gyration were determined after the stationary mode was established. The oscillating mean magnetic moment in each disc was characterized by a complex quantity

$$m_n = m_{nx} + im_{ny}, \tag{7}$$

where m_n is the induced magnetic moment in the first and second discs ($n = 1,\ 2$). The phase difference of oscillations in discs was calculated as

$$\Delta\varphi_{12} = \text{Arg}(m_1) - \text{Arg}(m_2). \tag{8}$$

The oscilloscope records of phase difference oscillations for steady gyrotropic oscillations of vortices in neighboring discs are presented in Figure 9. The amplitude of phase oscillation in the H^+H^+/V^+V^+ and H^+H^+/V^-V^- configurations (Figure 9, a) was 0.90° and 0.72°, respectively. In the H^+H^+/V^+V^- configuration, oscillation synchronization was not observed due to a significant difference in partial frequencies of the gyrotropic vortex mode in magnetic fields (Figure 9, b). At the same time, when the pump currents in adjacent discs were oppositely

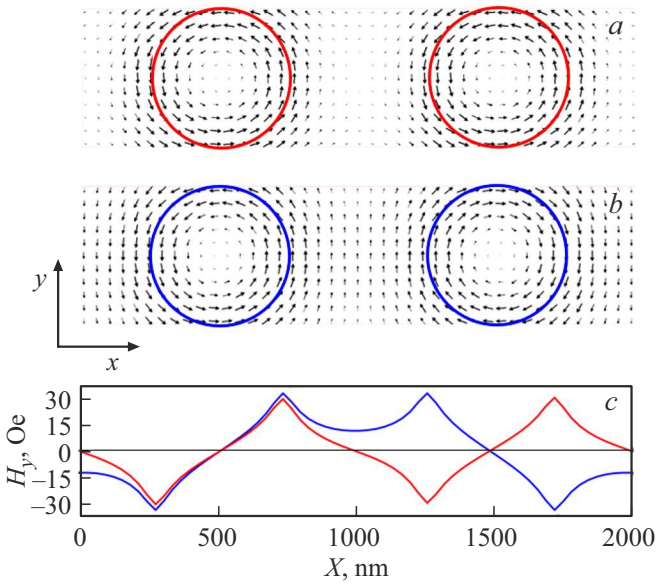

Figure 8. *a*) Spatial structure of the H^+H^+ magnetic field with the pump current having the same direction in adjacent discs. (*b*) Structure of the H^+H^- field in the case when the pump current has different directions in adjacent discs. *c*) Corresponding distributions of the *Y*-amplitude of fields in the cross section of a cell. The red and blue curves correspond to the H^+H^+ and H^+H^- configurations, respectively.

directed, oscillation synchronization with very weak phase oscillations (at the $10^{-5\circ}$ level, which is close to the error of numerical integration; see Figure 9, *c*) was observed for the H^+H^-/V^+V^- and H^+H^-/V^-V^+ configurations. In the H^+H^-/V^+V^+ configuration, synchronization was also not observed (Figure 9, *d*).

The amplitudes of phase difference oscillations for different configurations of vortices and magnetic fields are listed in the table for comparison (lack of synchronization is denoted by $-$)).

It follows from the results of earlier studies that a reduction in the distance between discs in the chain leads to a significant enhancement of magnetostatic [16] and exchange [21] coupling (when discs start to overlap). It would seem that this enhanced coupling could lead to synchronization in the H^+H^+/V^+V^- and H^+H^-/V^+V^+ configurations. However, simple calculations of the magnetic field of spin-polarized current reveal the emergence of significant distortions in the field configuration within the discs due to the mutual influence of magnetic fields of adjacent discs. In other words, the Oersted field in each disc will become eccentric, and a magnetic vortex with its core at the geometric center of a disc will no longer be the equilibrium state of the system. This field distribution will induce significant non-isochronism of gyrotropic motion of the vortex core and result in

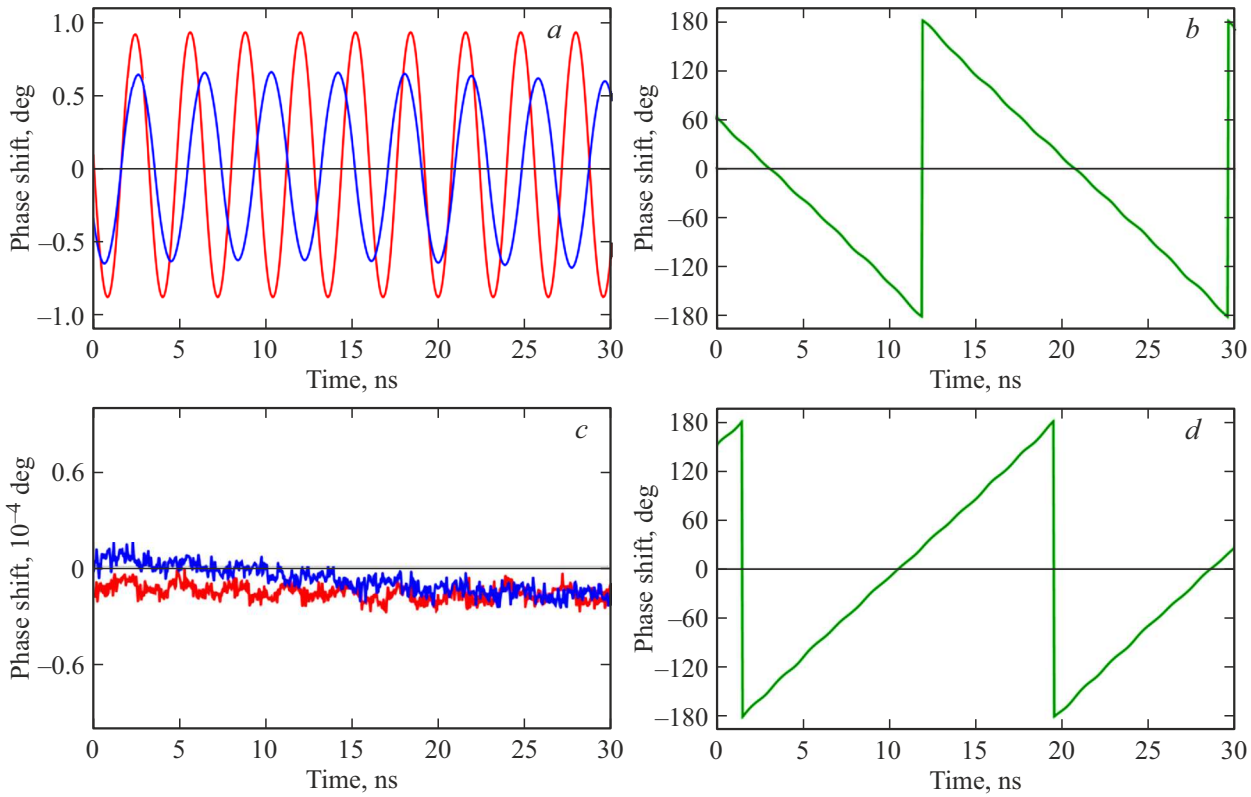

Figure 9. Oscilloscope records of the steady phase difference of oscillations of magnetic vortices in adjacent discs. *a*) Configurations H^+H^+/V^+V^+ (red curve) and H^+H^+/V^-V^- (blue curve); *b*) configuration H^+H^+/V^+V^-, no synchronization; *c*) configurations H^+H^-/V^+V^- (red curve) and H^+H^-/V^-V^+ (blue curve); *d*) configuration H^+H^-/V^+V^+, no synchronization.

Amplitude of phase difference oscillations for different configurations of magnetic fields and magnetic vortices

Field	Vortex	Phase
H^+H^+	V^+V^+	0.90°
H^+H^+	V^-V^-	0.72°
H^+H^+	V^+V^-	(−)
H^+H^-	V^+V^-	0.00°
H^+H^-	V^-V^+	0.00°
H^+H^-	V^+V^+	(−)

the lack of frequency synchronization. Note that similar negative synchronization effects will be observed for all four disc vorticity configurations and current flow directions. Therefore, one should produce chains with a certain optimal distance at which the magnetostatic interaction is already sufficient for synchronization but the negative influence of the Oersted field eccentricity does not manifest itself.

5. Conclusion

It was demonstrated via micromagnetic modeling that the magnetic field of pump current exerts a significant influence on the parameters of gyrotropic self-oscillations of a magnetic vortex in a ferromagnetic disc. To minimize this effect, one needs to reduce the thickness of supply electrodes and compensate for the magnetic fields of supply wires. It was found that the pump current field affects the H^+/V^+ and H^+/V^- states differently, increasing the gyration frequency in one case and reducing it in the other. This is crucial for synchronization of gyrotropic self-oscillations in chains of interacting discs. The results of micromagnetic modeling of gyrotropic self-oscillations in disc chains revealed that the best conditions for synchronization are established in the H^+H^-/V^+V^- and H^+H^-/V^-V^+ configurations with pump currents directed oppositely. Such systems may be constructed based on arrays of discs coupled with nanowires [33].

Funding

This study was carried out under the state assignment of the Institute of Applied Physics, Russian Academy of Sciences (project No. FFUF-2024-0021).

Conflict of interest

The authors declare that they have no conflict of interest.

References

[1] N.A. Usov, L.G. Kurkina. J. Magn. Magn. Mater. **242**–**245**, *Part 2*, 1005 (2002).
[2] K.Yu. Guslienko, B.A. Ivanov, V. Novosad, Y. Otani, H. Shima, K. Fukamichi. J. Appl. Phys. **91**, *10*, 8037 (2002).
[3] J.P. Park, P. Eames, D.M. Engebretson, J. Berezovsky, P.A. Crowell. Phys. Rev. B **67**, *2*, 020403 (2003).
[4] K.Yu. Guslienko, X.F. Han, D.J. Keavney, R. Divan, S.D. Bader. Phys. Rev. Lett. **96**, *6*, 067205 (2006).
[5] S.-B. Choe, Y. Acremann, A. Scholl, A. Bauer, A. Doran, J. Stöhr, H.A. Padmore. Sci. **304**, *5669*, 420 (2004).
[6] V. Novosad, F.Y. Fradin, P.E. Roy, K.S. Buchanan, K.Y. Guslienko, S.D. Bader. Phys. Rev. B **72**, *2*, 024455 (2005).
[7] B. Pigeau, G. de Loubens, O. Klein, A. Riegler, F. Lochner, G. Schmidt, L.W. Molenkamp, V.S. Tiberkevich, A.N. Slavin. Appl. Phys. Lett. **96**, *13*, 132506 (2010).
[8] X. Cui, S. Yakata, T. Kimura. IEEE Trans. Magn. **51**, *11*, 4300303 (2015).
[9] V.L. Mironov, E.V. Skorokhodov, D.A. Tatarskiy, I.Yu. Pashen'kin. Tech. Phys. **65**, *11*, 1740 (2020).
[10] G. Hrkac, D. Hahn, L. Saharan, T. Schrefl, J.-V. Kim, T. Devolder, C. Chappert. IEEE Trans. Magn. **48**, *11*, 3811 (2012).
[11] V. Pribiag, I. Krivorotov, G. Fuchs, P.M. Braganca, O. Ozatay, J.C. Sankey, D.C. Ralph, R.A. Buhrman. Nature Phys. **3**, *7*, 498 (2007).
[12] A. Dussaux, B. Georges, J. Grollier, V. Cros, A.V. Khvalkovskiy, A. Fukushima, M. Konoto, H. Kubota, K. Yakushiji, S. Yuasa, K.A. Zvezdin, K. Ando, A. Fert. Nature Commun. **1**, *1*, 8 (2010).
[13] F.B. Mancoff, N.D. Rizzo, B.N. Engel, S. Tehrani. Nature **437**, *7057*, 393 (2005).
[14] F.A. Araujo, A.D. Belanovsky, P.N. Skirdkov, K.A. Zvezdin, A.K. Zvezdin, N. Locatelli, R. Lebrun, J. Grollier, V. Cros, G. de Loubens, O. Klein. Phys. Rev. B **92**, *4*, 045419 (2015).
[15] N. Locatelli, A. Hamadeh, F. Abreu Araujo, A.D. Belanovsky, P.N. Skirdkov, R. Lebrun, V.V. Naletov, K.A. Zvezdin, M. Munoz, J. Grollier, O. Klein, V. Cros, G. de Loubens. Sci. Rep. **5**, *1*, 17039 (2015).
[16] A.D. Belanovsky, N. Locatelli, P.N. Skirdkov, F. Abreu Araujo, K.A. Zvezdin, J. Grollier, V. Cros, A.K. Zvezdin. Appl. Phys. Lett. **103**, *12*, 122405 (2013).
[17] S. Kaka, M.R. Pufall, W.H. Rippard, T.J. Silva, S.E. Russek, J.A. Katine. Nature **437**, *7057*, 389 (2005).
[18] S. Erokhin, D. Berkov. Phys. Rev. B **89**, *14*, 144421 (2014).
[19] A. Ruotolo, V. Cros, B. Georges, A. Dussaux, J. Grollier, C. Deranlot, R. Guillemet, K. Bouzehouane, S. Fusil, A. Fert. Nature Nanotechnol. **4**, *8*, 528 (2009).
[20] Q. Zhu, Q. Zheng, X. Liu, J. Wang, Q. Liu. J. Appl. Phys. **117**, *17*, 173907 (2015).
[21] D.A. Tatarskiy, V.L. Mironov, A.A. Fraerman. JETP **136**, *3*, 321 (2023).
[22] Y.-S. Choi, S.-K. Kim, K.-S. Lee, Y.-S. Yu. Appl. Phys. Lett. **93**, *18*, 182508 (2008).
[23] V. Khvalkovskiy, J. Grollier, A. Dussaux, K.A. Zvezdin, V. Cros. Phys. Rev. B **80**, *14*, 140401(R) (2009).
[24] A. Dussaux, A.V. Khvalkovskiy, P. Bortolotti, J. Grollier, V. Cros, A. Fert. Phys. Rev. B **86**, *1*, 014402 (2012).
[25] H. Bhoomeeswaran, P. Sabareesan. SPIN **10**, *2*, 2050012 (2020).
[26] F. Abreu Araujo, C. Chopin, S. de Wergifosse. Sci. Rep. **12**, *1*, 10605 (2022).

[27] A. Vansteenkiste, J. Leliaert, M. Dvornik, M. Helsen, F. Garcia-Sanchez, B. Van Waeyenberge. AIP Advances **4**, *10*, 107133 (2014).
[28] J.C. Slonczewski. J. Magn. Magn. Mater. **159**, *1–2*, L1 (1996).
[29] J. Xiao, A. Zangwill, M.D. Stiles. Phys. Rev. B **70**, *17*, 172405 (2004).
[30] G.S. Abo, Y.K. Hong, J. Park, J. Lee, W. Lee, B.C. Choi. IEEE Trans. Magn. **49**, *8*, 4937 (2013).
[31] M. Noske, H. Stoll, M. Fähnle, A. Gangwar, G. Woltersdorf, A. Slavin, M. Weigand, G. Dieterle, J. Förster, C.H. Back, G. Schütz. Phys. Rev. Lett. **117**, *3*, 037208 (2016).
[32] K.Yu. Guslienko, K.-S. Lee, S.-K. Kim. Phys. Rev. Lett. **100**, *2*, 027203 (2008).
[33] D.A. Tatarskiy, E.V. Skorokhodov, O.L. Ermolaeva, V.L. Mironov, A.A. Fraerman. Chirality Control of Magnetic Vortices in Ferromagnetic Disk–Nanowire System. J. Surf. Invest.: X-Ray, Synchrotron Neutron Tech. **18**, *3*, 671 (2024).

Translated by D.Safin